Particle-in-Cell Simulation of Electron and Ion Energy Distributions in dc/rf Hybrid Capacitively-Coupled Plasmas

Paola Diomede

Plasma Processing Laboratory, Dept. of Chemical and Biomolecular Engineering, University of Houston, Houston, TX 77204

Doosik Kim

Process Technology Modeling, Design and Technology Solutions, Intel Corp., Hillsboro, OR 97124

Demetre J. Economou

Plasma Processing Laboratory, Dept. of Chemical and Biomolecular Engineering, University of Houston, Houston, TX 77204

A Particle-in-Cell simulation with Monte Carlo collisions was used to study electron and ion energy distributions (IEDs) in low-pressure (2.67 Pa) direct-current (dc)/radio-frequency (rf) hybrid capacitively-coupled Ar plasmas. One electrode (dc/rf electrode) of the parallel plate diode was powered by a 13.56 MHz source, and a negative dc bias voltage, whereas the opposite (substrate) electrode was grounded. Secondary electrons emitted from the dc/rf electrode accelerated in the adjacent sheath and entered the plasma, yielding a high-energy tail of the electron energy distribution. For given dc bias voltage, the plasma density increased as the secondary electron emission yield due to ion bombardment increased. A fraction of the secondary electrons were energetic enough to overcome the sheath potential barrier on the substrate electrode and bombard the substrate. The electron angular distribution on the substrate electrode had a peak of directional electrons superimposed on a typical cosine distribution. The mean energy and angular spread of directional electrons could be controlled by varying the dc bias voltage. However, as the dc bias became more negative, the dc/rf sheath expanded at the expense of the bulk plasma, reducing the plasma density, in agreement with published data. The IED on the substrate electrode exhibited a dominant bimodal feature with multiple shoulder peaks due to ion-neutral charge exchange collisions. The average ion energy decreased as the dc voltage became more negative, also in agreement with data. Pulsing the plasma power enhanced the tail of the electron energy distribution in the early activeglow (power ON), and yielded a distinct ballistic electron flux on the substrate with energy equal to the applied dc bias. © 2013 American Institute of Chemical Engineers *AIChE J*, 59: 3214-3222, 2013

Keywords: plasma, simulation, molecular, energy distribution

Introduction

Radio-frequency (rf) capacitively-coupled plasmas (CCP) are widely used in microelectronic device fabrication for plasma etching and deposition of thin films.[1] In plasma etching, energetic electrons create reactive radicals and ions by dissociation and ionization of a feedstock gas. Radicals adsorb and react on the wafer surface to produce volatile products, thereby etching a film. Anisotropic (vertical) etching is obtained when the surface reaction is induced by high-energy (100 s of eV) positive ion bombardment. Positive ions gain directional energy in the sheath that forms over any surface in contact with plasma. In plasma deposition, radicals adsorb and react on the surface to deposit a film. The deposition rate and the film microstructure and proper-

ties are greatly influenced by low-energy (10 s of eV) ion bombardment.

As integrated circuit features continue to shrink, approaching atomic dimensions, precise and independent control of the energy and angular distributions of plasma species becomes increasingly more important.[2] Specifically, the electron energy distribution function (EEDF) dictates gas ionization and radical production rates, whereas the ion energy distribution (IED) at the wafer drives surface reaction rates. The ion energy must be high enough to achieve anisotropic etching, but not too high to cause loss of selectivity or substrate damage. Selectivity refers to etching the desired film while not etching another, for example, the mask or the underlying substrate. Dual frequency plasma sources have been used to (quasi)-independently control the energy and flux of *ions* impinging on the wafer.[3] High-frequency power is used for plasma production to control ion flux (also radical flux), whereas low-frequency power is used for ion acceleration in the sheath, to control ion energy. A more recent

development is the use of a direct-current (dc) voltage to bias one of the electrodes of an otherwise conventional parallel plate CCP, to control not only the *electron* energy distribution in the plasma, but especially the energy and angular distributions of electrons and ions bombarding a wafer on the substrate electrode.[4–11] The first application of a dc bias to a conventional rf CCP reactor appears to have been published in 1985.[4]

Recent studies of this dc/rf hybrid plasma source showed that secondary electron emission from the dc electrode and subsequent acceleration of these electrons in the adjacent sheath electric field could result in a beam of ballistic electrons striking the wafer on the opposite electrode.[4–9] The energy and directionality of the electron beam may be controlled by varying the dc bias voltage. The term "ballistic" refers to directional electrons, of relatively high-energy (100 s of eV), that can cross the interelectrode gap without collisions. The electron impact collision cross sections decrease with energy at high energies (see Ref. 1, p. 73). This fact, coupled with the low-pressure, makes the mean free path of ballistic electrons larger than the interelectrode gap. It was suggested that this energetic and directional electron beam could reduce differential charging of microfeatures on the wafer surface, ameliorating undesired etch artifacts, such as twisting or notching, in high aspect ratio (70:1) submicron diameter holes etched in dielectrics.[10,12] Differential charging of (insulating) features (trenches, holes) can occur because, in a conventional plasma reactor, the velocity distribution of electrons striking the wafer surface is nearly isotropic, whereas positive ions have a strongly anisotropic velocity distribution, peaked perpendicular to the wafer. Thus, positive ions can reach the bottom of the feature, charging it positively, whereas electrons dissipate near the entrance of the feature, charging it negatively. This differential charging, and the resulting electric field, divert further oncoming ions off the vertical, leading to undesirable etching artifacts. A directional flux of high-energy electrons can penetrate to the bottom of the feature, neutralizing the positive charge, thus reducing differential charging.

In this work, a Particle-in-Cell simulation coupled with Monte Carlo collisions (PIC-MCC) was used to investigate the electron energy and angular distributions, as well as the IEDs, in a dc/rf hybrid parallel-plate Ar CCP discharge. Emphasis was placed on the effect of secondary electron yield (SEY) by ion bombardment. Next, a brief description of the reactor configuration and the PIC-MCC simulation approach is followed by Results and Discussions, ending with Summary and Conclusions.

Simulation Model

Plasma reactor

The dc/rf hybrid CCP reactor investigated in this study is shown schematically in Figure 1. It was a parallel-plate diode with an interelectrode gap of 0.05 m. The background Ar gas was uniform at 2.67 Pa and 500 K. The electrode at $x = 0$ (henceforth called the "dc/rf electrode") was powered by a rf source [$V_{rf} \sin(2\pi vt)$, where $v = 13.56$ MHz], and a negative dc bias. A substrate wafer would rest on the grounded counter-electrode (henceforth called the "substrate electrode") at $x = 0.05$ m. Both dc and rf sources were voltage-controlled with $V_{rf} = 500$ V and variable V_{dc}. The base case condition was $V_{dc} = -200$ V. Ion impact caused emission of
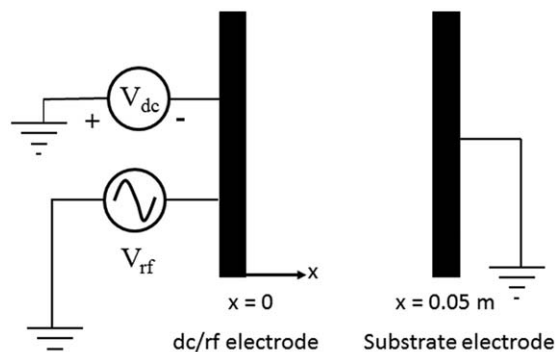

Figure 1. Schematic diagram of a dc/rf hybrid capacitively-coupled plasma.

The left (dc/rf) electrode ($x = 0$) was powered by a 13.56 MHz voltage source ($V_{rf} = 500 \sin(2\pi vt)$ in V, $v = 13.56$ MHz), and a negative dc bias voltage (V_{dc}), whereas the opposite (substrate) electrode ($x = 0.05$ m) was grounded. The interelectrode gap was 0.05 m. The working gas was Ar at 2.67 Pa and 500 K. Base case condition was $V_{dc} = -200$ V. The secondary electron emission yield due to ion bombardment is designated as γ_{sec}.

secondary electrons from both electrodes. The SEY was varied between 0.0 and 0.3. (SEY is the number of electrons emitted per ion striking the surface.) The SEY was taken independent of the energy of impacting ions.[9] Emission of secondary electrons due to electron bombardment was not included in this study.

PIC-MCC simulation

The plasma particle (electrons, ions, neutrals) dynamics can be described by the Boltzmann equation in the 7-D coordinate system of phase space ($\mathbf{x}$, $\mathbf{v}$) plus time, t.

$$\frac{\partial f}{\partial t} + \mathbf{v} \cdot \frac{\partial f}{\partial \mathbf{x}} + \frac{\mathbf{F}}{m} \cdot \frac{\partial f}{\partial \mathbf{v}} = \left(\frac{\partial f}{\partial t}\right)_{coll} \tag{1}$$

Here, $\mathbf{x}$ and $\mathbf{v}$ are particle (vector) location and velocity, respectively, and f is the particle distribution function. The right-hand side of Eq. 1 is the collision operator. $\mathbf{F} = q(\mathbf{E} + \mathbf{v} \times \mathbf{B})$ is the Lorentz force acting on a particle with charge q. The Lorentz force is generally found by solving Maxwell's equations for the electric field $\mathbf{E}$ and the magnetic induction $\mathbf{B}$. In the present work, the problem is electrostatic, hence $\mathbf{B} = 0$.

The PIC-MCC simulation essentially solves the Boltzmann Eq. 1. In this work, the simulation was $1d3v$, that is, in one spatial dimension (perpendicular to the electrodes) but with all three velocity components of the computational particles accounted for.[13–16] Computational particles (superparticles) were tracked over a mesh with appropriate initial conditions. Particles moved according to Newton's equation of motion,

$$\begin{aligned} \frac{d\mathbf{x}}{dt} &= \mathbf{v} \\ \frac{d\mathbf{v}}{dt} &= \frac{\mathbf{F}}{m} \end{aligned} \tag{2}$$

At the end of the particle motion time step, Monte Carlo collisions were executed (Figure 2). The null-collision
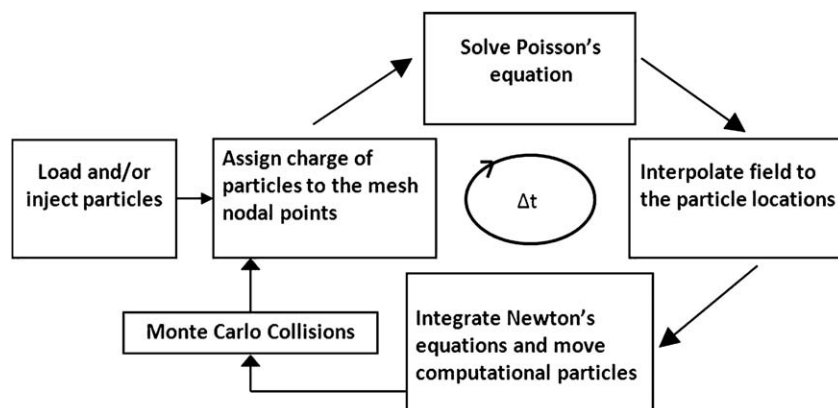
Figure 2. Flow chart of the Particle-in-Cell Monte Carlo Collisions (PIC-MCC) simulation procedure.

technique was used for computational efficiency.[15] Elastic, excitation, and ionization collisions of electrons with Ar gas were taken into account. Elastic scattering and charge exchange collisions of Ar^+ ions with background neutrals were also included.[15,17] After the Monte Carlo step, the charge of each particle was distributed to the nodal points of the computational mesh using bilinear interpolation. Based on the resulting charge density, Poisson's equation was solved and the electric field was calculated at the nodal points. The electric field was then interpolated at the location of the particles using a bilinear function. The new electric field gave a new Lorentz force on the particles for the next motion time step. The cycle was repeated (Figure 2) until a periodic steady-state was reached, and the statistics were adequate to calculate the electron and ion distribution functions as well as the potential distribution.

An argon plasma containing a single ion species (Ar^+) and electrons was simulated. An explicit, time-centered leap frog method[13] was used for integration of Eq. 2, obeying the Courant condition, $(v\Delta t/\Delta x) < 1$, where v is the particle speed, and Δt and Δx are the time step and grid cell size, respectively. The simulation used 300 equally-sized cells to represent the 0.05 m-long discharge region. A total of about 10^5 superparticles were used to minimize statistical fluctuations. Time marching continued until a periodic steady-state was achieved after ~1000 rf cycles. The simulation predicted the density as well as the energy and angular distributions of electrons and ions as a function of position between the plates and on the electrode surfaces.[18-20]

Results and Discussions

Figure 3 shows time-average ion (solid lines) and electron (dashed lines) density profiles for the base case condition. The SEY (γ_{sec}) was varied from 0 to 0.3. The case of no dc bias (rf only) and SEY = 0 is also shown. The density profiles in the bulk plasma are "diffusion like." The ion and electron density are very nearly equal in the bulk plasma (electro-neutrality) but deviate in the sheath, which contains a net positive charge. The sheath edge was defined as the point where the relative difference between ion and electron density was $(n_i - n_e)/n_i = 0.01$. For $V_{dc} = 0$, the density profile is symmetric with respect to the central plane. When a negative dc voltage is applied, the profile becomes asymmetric. For given rf and dc voltages, the plasma density increases (and the sheath becomes thinner) as the SEY

increases. Similar observations were reported by other researchers.[7] Ion bombardment of the electrodes creates secondary electrons that accelerate in the sheath and stream back into the plasma. Despite their low density, these highly energetic secondaries can produce ionization, even at the relatively low-pressure of 2.67 Pa, leading to considerable increase (almost 2X) of plasma density, as the SEY increases from 0.0 to 0.3. For given value of SEY, the peak plasma density decreases when a dc bias is applied. This will be discussed later.

The dc bias modifies the sheath structure. As shown in Figure 3, the dc/rf sheath (adjacent the left electrode) is thicker than the rf sheath. When a negative dc bias is applied on the electrode, an electron-free dc sheath is added to the rf sheath of an otherwise symmetrical rf CCP. Due to the dc bias, the dc/rf sheath has a larger potential drop than the rf sheath on the opposite (substrate) electrode. Figure 4 shows waveforms of the two sheath potentials (the sheath potential was approximated as the bulk plasma [at $x = 0.025$ m] potential minus the electrode potential) over two rf cycles for the base case condition, with SEY = 0.2. The maximum sheath potential is 710 V for the dc/rf sheath but only 350 V for the rf sheath. The dc/rf sheath potential is almost
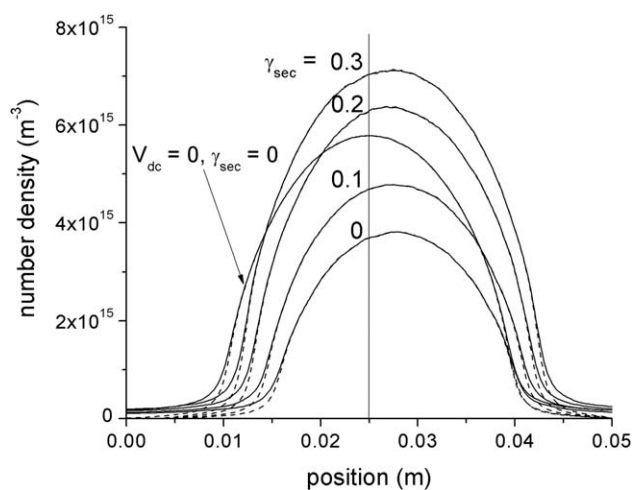

Figure 3. Time-average ion (solid lines) and electron (dashed lines) density profiles for $V_{dc} = -200$ V.

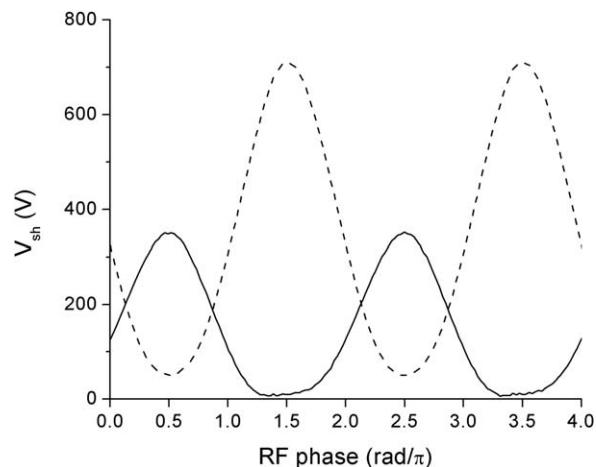Secondary electron emission yield due to ion bombardment was varied.

Figure 4. Waveforms of dc/rf (dashed line) and rf (solid line) sheath potentials over two rf cycles. The secondary electron emission yield was fixed at 0.2. $V_{dc} = -200$ V.

Figure 5. Time-average electron energy probability functions at the discharge center ($x = 0.025$ m) for $V_{dc} = -200$ V.

Secondary electron emission yield due to ion bombardment was varied.

sinusoidal but the rf sheath potential displays nonlinear flattening for a considerable fraction of the rf cycle.

In the absence of collisions with the background gas, the kinetic energy that secondary electrons gain in the sheath is equal to the sheath potential at the time the electron is produced at the wall. This is because the electron sheath transit time is much shorter than the rf period. Inelastic collisions with the background gas reduce the electron energy. However, the mean free path of electron impact ionization of Ar, by say 300 eV electrons (cross section = 1.98 10^{-20} m^2), is about 0.05 m at 2.67 Pa and 500 K, resulting in a probability of electrons reaching the rf electrode without ionizing of 0.37. In any case, since each ionizing collision consumes only about 20 eV,[6] secondary electrons retain most of the kinetic energy gained in the sheath, populating the high-energy tail of the EEDF.

Figure 5 depicts the electron energy probability function (EEPF) at the discharge center ($x = 0.025$ m) as the SEY is increased under otherwise the base case condition. A Maxwellian EEPF would be a straight line on this plot. Without secondary electrons (SEY = 0), the EEPF has a bi-Maxwellian (two distinct slopes) character. Secondary electron production boosts the high-energy tail of the distribution, more so as SEY increases. The EEPFs display two shoulder features when secondary electrons are present. These features are located at ~710 eV and ~350 eV, corresponding to the maximum potential of the dc/rf sheath and rf sheath, respectively (Figure 4). These maxima occur at $\omega t = 3\pi/2$ for the dc/rf sheath and $\pi/2$ for the rf sheath. The sheath potentials change relatively slowly during these phases of the rf cycle, resulting in a larger fraction of electrons possessing the respective energies, which explains the appearance of the slight peaks. Secondary electrons continue to be produced throughout the rf cycle populating the whole energy range in the tail of the EEPF. The EEPF enhancement in a range from 350 eV to 710 eV is due to secondary electron emission from the dc/rf electrode. Secondary electrons from the rf electrode boost the EEPF below 350 eV.

Unlike bulk thermal electrons, secondary electrons are highly directional since they gain their kinetic energy accelerating in a strong one-dimensional (1-D) sheath electric field. Af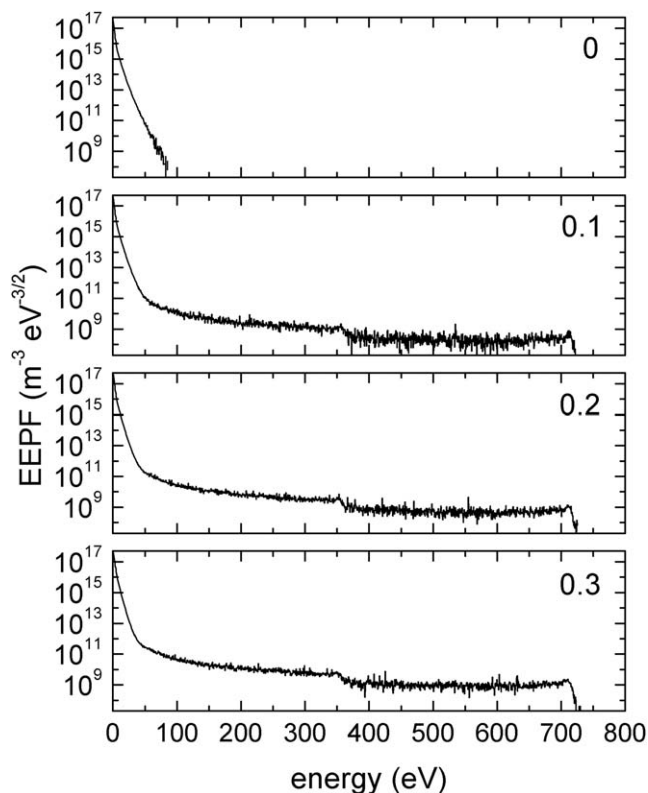ter crossing the plasma, secondaries face a potential barrier at the opposite electrode sheath. If the secondaries have enough energy to overcome that barrier, they will strike the electrode or a wafer resting on that electrode. Figure 6 shows the time-average angular distribution of electrons striking the substrate electrode for the base case condition. The cosine distribution is shown at the top as a reference. The simulation predicts a peak of directional electrons superimposed on an otherwise roughly cosine distribution. Ignoring collisions and sheath transit time, most of the secondary electrons produced at the dc/rf electrode have enough energy to strike the substrate electrode on a single pass (Figure 4). The peak of these "ballistic" electrons grows and tends to become sharper as the SEY increases. The angle of impact of the directional electrons is a few degrees off the normal direction.

Secondary electron emission also influences the IED, albeit not as much as the EEDF. The IED depends, among other variables, on the sheath voltage and the applied frequency. For a sinusoidal voltage and a collisionless sheath, the relevant parameter is $\frac{\tau_i}{\tau_{rf}} = \frac{3s\omega}{2\pi}\left(\frac{M}{2eV_s}\right)^{1/2}$ the ratio of the ion transit time through the sheath, τ_i, to the period of the applied rf, τ_{rf}.[21-23] Here, s, ω, M, and V_s are time-average sheath thickness, applied voltage angular frequency, ion mass, and time-average sheath voltage, respectively. When $\tau_i/\tau_{rf} \ll 1$, ions respond to the instantaneous sheath voltage, and the IED has a large energy spread, up to the maximum sheath potential. When $\tau_i/\tau_{rf} \gg 1$, ions respond to an average ("damped") sheath voltage, and the energy spread of the IED becomes narrow.

Figure 7 shows time-average IEDs at the substrate electrode for different values of the SEY. The maximum ion
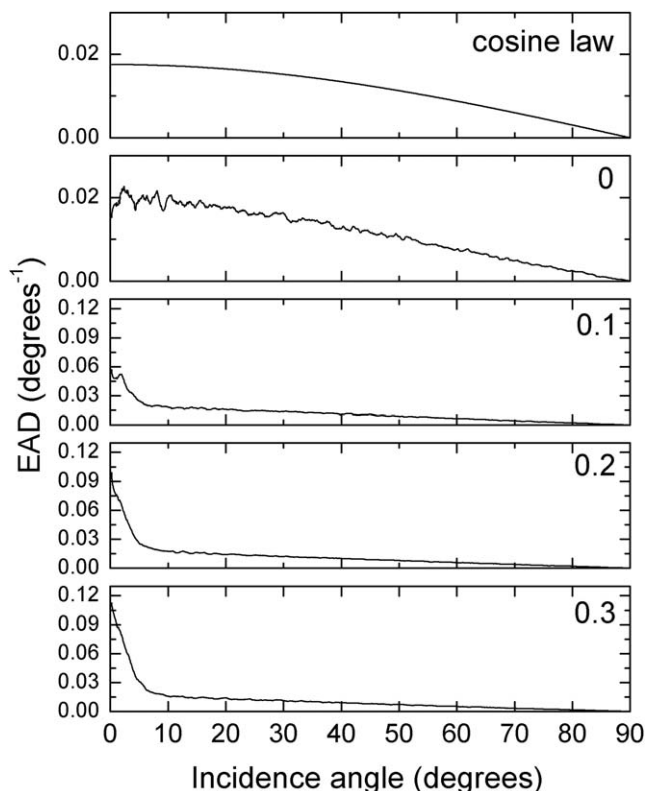
Figure 6. Time-average angular distribution of electrons bombarding the substrate electrode for $V_{dc} = -200$ V.

Secondary electron emission yield due to ion bombardment was varied. The cosine distribution is shown at the top as a reference.
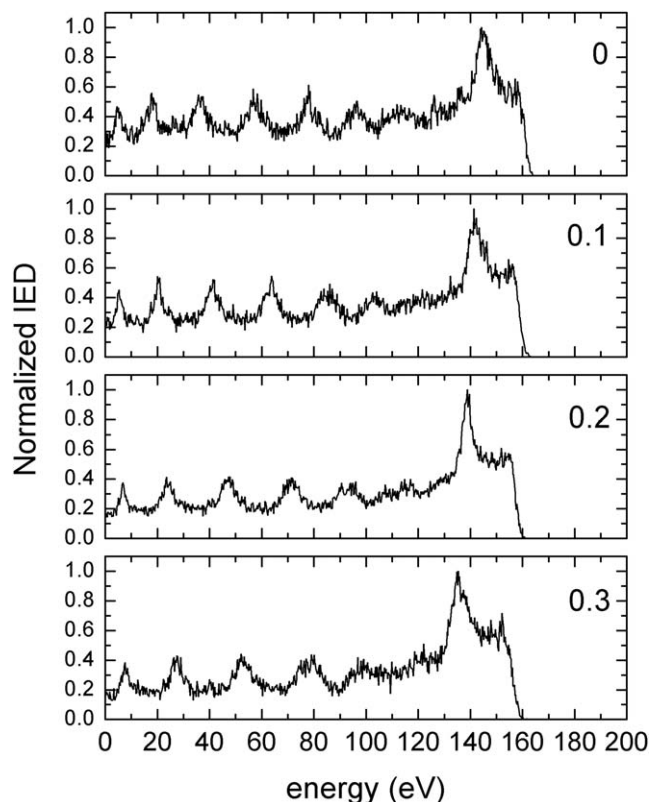

Figure 7. Time-average ion energy distribution function at the substrate electrode for $V_{dc} = -200$ V.

Secondary electron emission yield due to ion bombardment was varied.

energy is significantly lower than the peak potential of the respective sheath, indicating that ions do not respond to the rf field ($\tau_i/\tau_{rf} > 1$). The multiple peaks of the IED are due to charge exchange collisions.[24] As the SEY increases, the number of these peaks becomes smaller, because of reduced number of collisions in the (thinner) sheath.

The dc bias is a key parameter for controlling the electron kinetic energy. The time-average kinetic energy of electrons as a function of position in the interelectrode gap is shown in Figure 8. The average energy increases drastically when a dc bias is applied. In addition, the peak of the profile shifts away from the dc biased electrode as the sheath becomes thicker. The thicker sheath, however, results in reduced bulk plasma volume. Although secondary electrons accelerated in the sheath contribute to ionization of the gas, the main source of ionization is the much more populous bulk electrons. As the sheath thickens and the bulk plasma is "squeezed out," the overall ionization volume decreases resulting in lower plasma density as the dc bias becomes more negative. This is depicted in Figure 9 that shows time-average electron density profiles for different values of the dc voltage for fixed SEY = 0.2. More negative dc bias makes the electron-free sheath thicker and reduces the plasma density. Similar observations were reported by Jiang et al.[11] A decrease in the plasma density with the increase of the absolute value of the dc voltage is in agreement with experimental measurements of Zeuner et al.[25]

Figure 10 depicts the EEPF at the discharge center ($x = 0.025$ m) for SEY = 0.2 and varying V_{dc}. The tail of the

EEPF extends ∼20 eV beyond $V_{rf} + |V_{dc}|$, that is, the summation of the amplitude of the rf voltage and the absolute value of the dc voltage.[10,18]

Figure 11 shows the time-average angular distribution of electrons striking the substrate electrode for $V_{rf} = 500$ V, SEY = 0.2 and varying V_{dc}. Similar to Figure 6, a peak of directional electrons is superimposed on an otherwise roughly cosine distribution. The peak of "ballistic" electrons (at low incidence angles) appears even for $V_{dc} = 0$, since secondary electrons can still accelerate in a purely rf sheath.
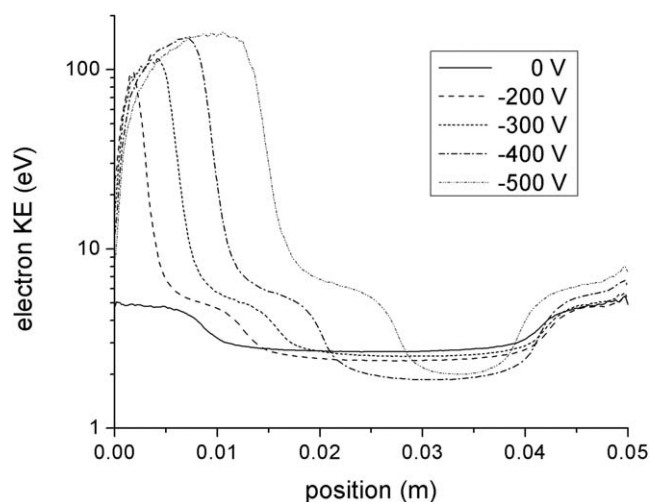

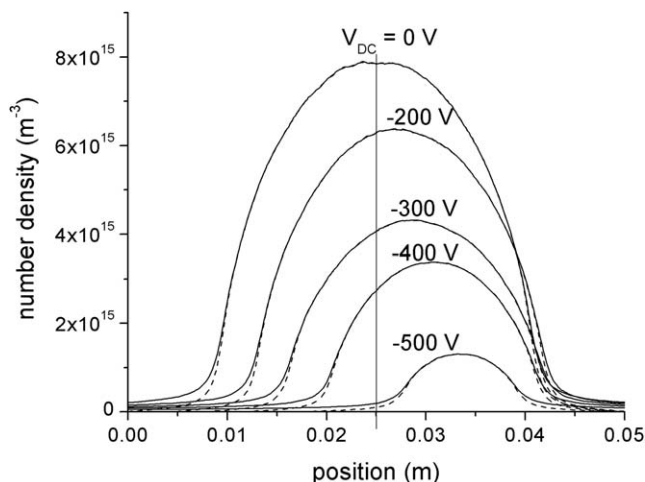**Figure 8. Time-average kinetic energy of electrons for SEY = 0.2. V_{dc} was varied from 0 to −500 V.**

Figure 9. Time-average ion (solid lines) and electron (dashed lines) density profiles for the conditions of Figure 8.

The peak height does not change significantly with V_{dc}. The ion density as well as the ion flux at the dc/rf electrode both decrease with more negative V_{dc} (Figure 9). This results in lower secondary electron flux leaving the dc/rf electrode. However, the sheath potential over the substrate electrode decreases with more negative V_{dc} (see below), allowing a larger fraction of the secondaries to reach that electrode, thus counterbalancing the lower secondary electron flux. The full width at half maximum of the peak appears to be reduced (sharper peak), as the dc bias becomes more nega-
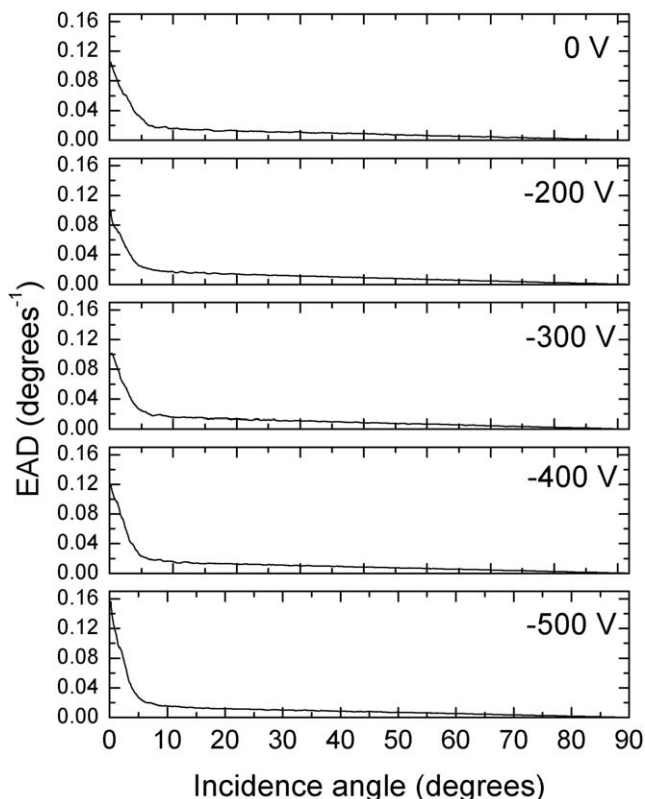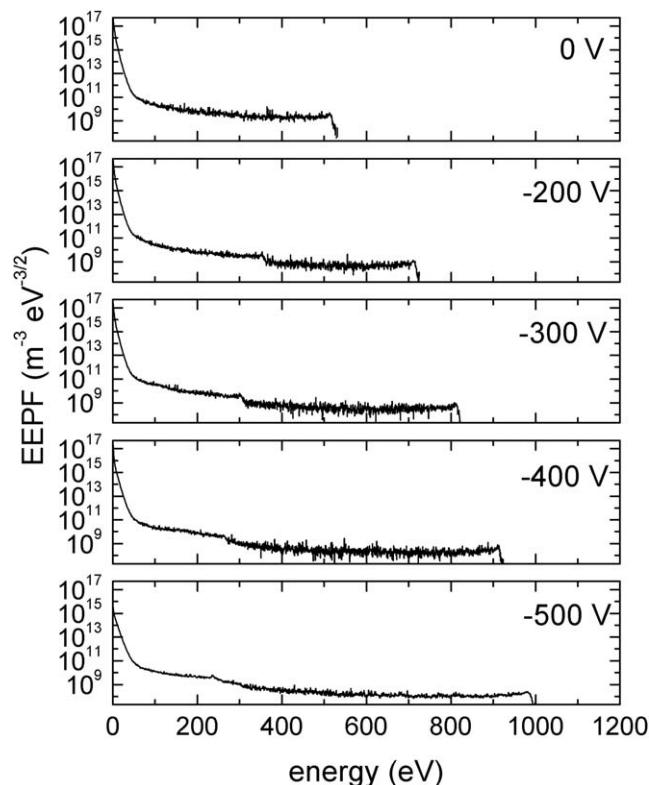

Figure 10. Time-average electron energy probability function (EEPF) at the discharge center ($x = 0.025$ m).

V_{dc} was varied from 0 to -500 V.

Figure 11. Time-average electron angular distribution at the substrate electrode for the conditions of Figure 8.

tive. This is because a more negative dc bias generates more directional electrons with higher energy. The collision cross section decreases at high energies, whereas the probability of forward scattering increases, resulting in more directional electron beam.

The dc bias has substantial influence on the IED as well (Figure 12). Both the average energy and the energy spread of the ions bombarding the substrate electrode are reduced as the dc bias becomes more negative. The electron particle current to the rf electrode increases, as the applied dc bias becomes more negative. This is because the dc bias expels electrons from the dc/rf electrode sheath and, to maintain charge neutrality in the plasma, these electrons have to escape through the substrate electrode. The potential of the substrate sheath decreases to allow these excess electrons to escape, with a concomitant decrease of the ion bombardment energy on the substrate electrode. The corresponding increase of the sheath width leads to an increase of the low energy secondary peaks, due to ions created by charge exchange collisions. A decrease in the maximum ion energy with the absolute value of the dc voltage was also observed experimentally.[25]

Pulsed plasma operation was also studied. The rf voltage driving the discharge was square-wave modulated with a frequency of 10 KHz and a duty ratio of 20%, that is., the voltage was turned ON at $t = 0$ and OFF at $t = 20$ μs, during each 100 μs period of pulsing. This resulted in roughly 20 μs of plasma-ON (active glow) and ~80 μs of plasma-OFF (afterglow) per cycle. A dc bias of -200 V was applied *continuously* on the powered electrode, and the SEY was set $= 0.2$. The simulation ran for 12 pulsed plasma cycles to achieve a periodic steady-state. Modulation of the discharge
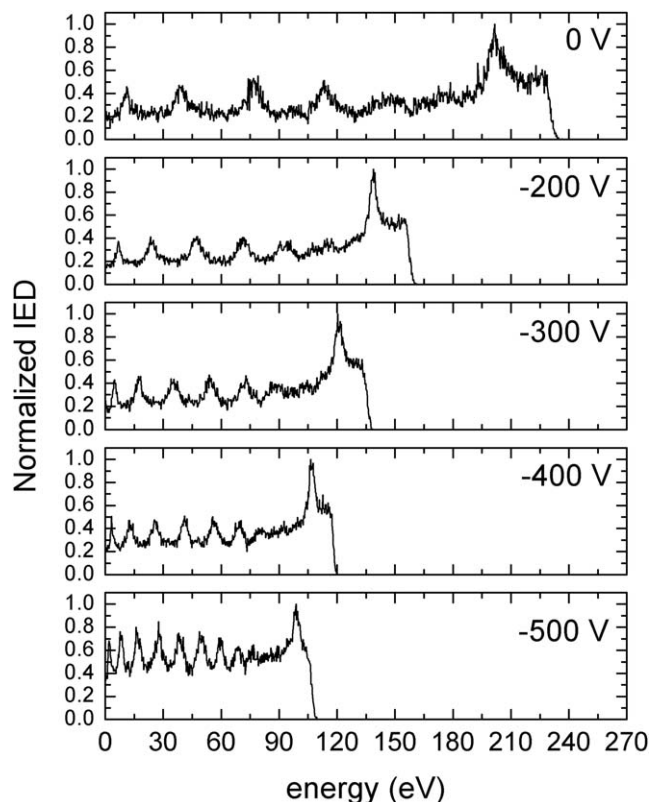
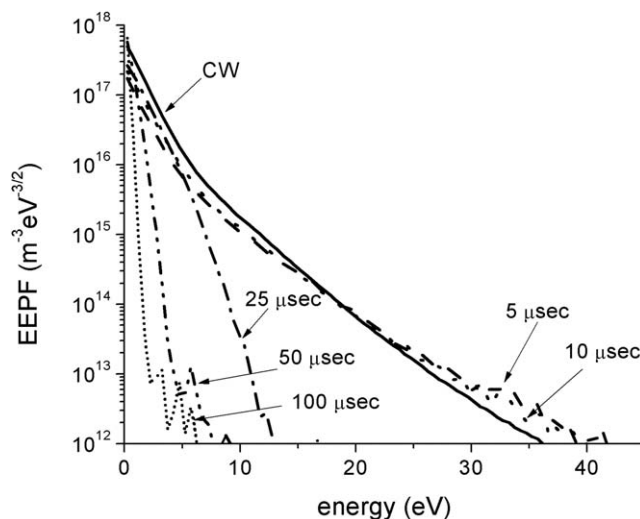Figure 12. Time-average ion energy distribution at the substrate electrode for the conditions of Figure 8.

Figure 13. Electron Energy Probability Function (EEPF) at the center of the discharge ($x = 0.025$ m), at different times during a cycle of a pulsed plasma.

The rf voltage ($V_{rf} = 500 \sin(2\pi\nu t)$) was pulsed at a frequency of 10 kHz (pulse period = 100 μs), with a duty cycle of 20%. The plasma was turned ON at $t = 0$ μs and OFF at $t = 20$ μs until $t = 100$ μs. SEY=0.2 and $V_{dc} = -200$ V. The EEPF for the corresponding continuous wave plasma is also shown.

has a direct effect on the EEPF. The EEPF at the central plane of the discharge ($x = 0.025$ m) as a function of time during a pulse is shown in Figure 13. Upon discharge turn ON, the tail of the EEPF extends to higher energies compared to the EEPF of a cw plasma, under otherwise identical conditions. This is due to stronger heating of the electron cloud by the oscillating sheath. Correspondingly, the number of low-energy electrons decreases. Therefore, pulsing of the plasma power provides additional "knobs" to control the EEPF, and in turn the plasma chemistry. In fact, the effect of plasma pulsing would have been more dramatic, should the voltage during plasma ON were adjusted upwards, to deposit the same amount of time-average power in the pulsed plasma, as in the cw plasma. Figure 13 shows that the EEPF cools down rapidly after plasma turn OFF at $t = 20$ μs. It turned out that, at a given spatial location, the tail of the EEPF was enhanced more for lower pulse repetition frequencies and/or shorter duty cycles.

The energy distribution of electrons bombarding the substrate electrode is shown in Figure 14. The time-average electron energy distribution (EED) of the pulsed plasma is compared to that of a cw plasma, under otherwise the same conditions. The EEDs are similar except that the pulsed plasma EED has a distinct peak at 200 V. This corresponds to the −200 dc bias applied on the powered electrode. When rf power to the plasma is turned off (in the afterglow), the rf electric fields disintegrate within several μs. However, the dc voltage is still on, accelerating electrons in the dc sheath. In the absence of gas-phase collisions, these electrons reach the substrate electrode with their full energy, since there is essentially no sheath over the substrate electrode to affect
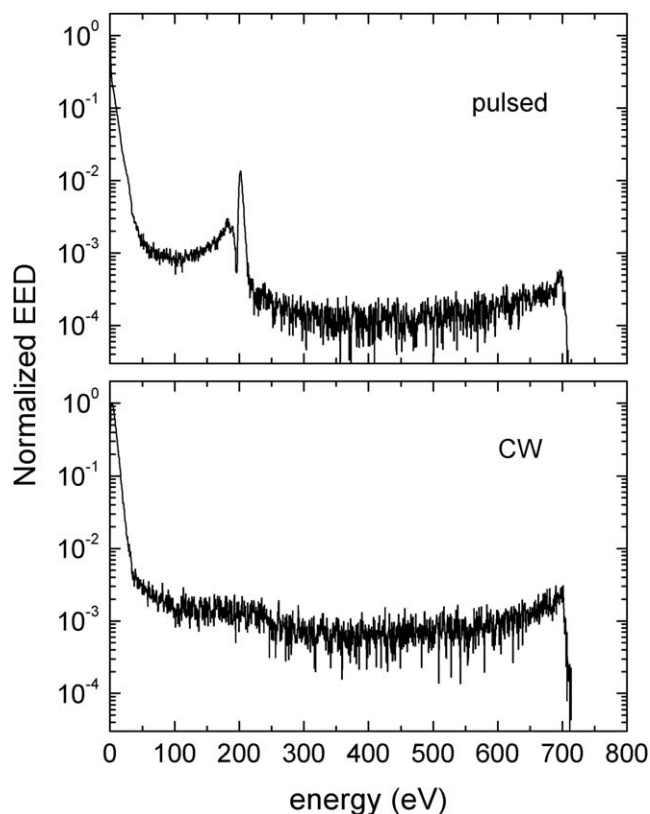

Figure 14. Top: Time-average electron energy distribution (EED) at the substrate for the pulsed plasma conditions of Figure 13.

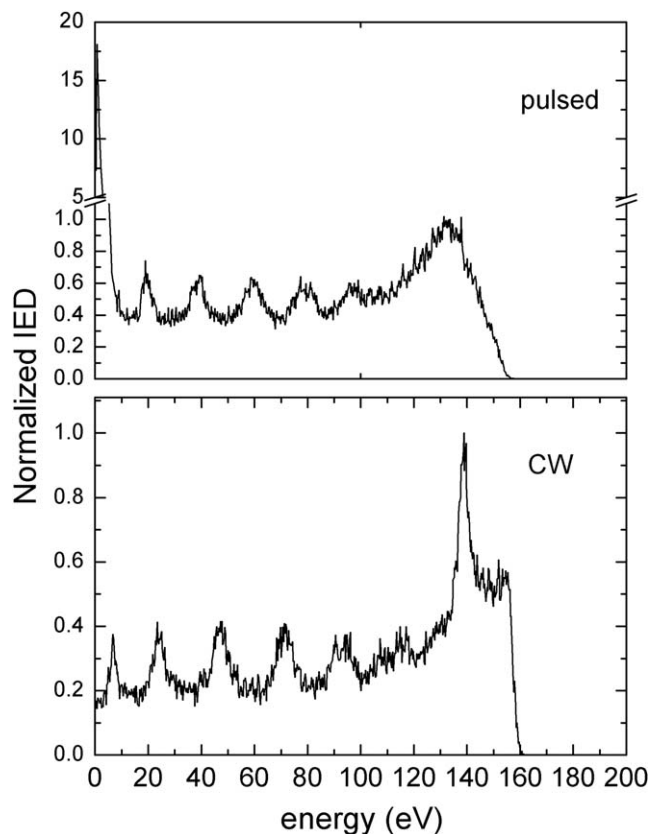Bottom: Corresponding EED for continuous wave plasma.

Figure 15. Top: Time-average ion energy distribution (IED) at the substrate for the pulsed plasma conditions of Figure 13.

Bottom: Corresponding IED for continuous wave plasma.

their motion. The time-average IED on the substrate electrode of a pulsed plasma is compared to that of a cw plasma in Figure 15. The IEDs are similar except for a very low-energy peak in the case of pulsed plasma. This peak corresponds to the ions striking the substrate during the rf power OFF phase of the cycle. As mentioned above, the sheath voltage disintegrates during the afterglow, giving rise to a flux of very low-energy ions. The high-energy feature of the IED is smeared out in the case of pulsed plasma because, during the afterglow, ions respond to an average sheath voltage.

Summary and Conclusions

A PIC-MCC simulation was used to investigate the effect of an externally applied negative dc bias on the electron and ion energy distributions (IEDs) in a low-pressure dc/rf hybrid capacitively-coupled Ar discharge. A directional energetic electron beam could result by secondary electrons emitted from the electrode biased with a high negative dc voltage. Secondary electrons were accelerated by the 1-D sheath electric field back into the plasma. Due to their long mean-free-path under the prevailing low-pressure, these "ballistic" electrons retained most of the kinetic energy gained in the sheath and were able to overcome the sheath potential barrier on the opposite (substrate) electrode holding the wafer. The angular spread of the ballistic electrons was only a few degrees off the normal to the wafer surface. It is believed that directional electrons can ameliorate differential charging of high aspect ratio features, thereby alleviating etch artifacts

such as twisting and notching. Application of a more negative dc bias increased the mean energy and decreased the angular spread of the ballistic electron beam. However, as the dc bias became more negative, the plasma density decreased due to a reduction in bulk plasma volume.

Plasma pulsing provided another way of controlling the EEPF. When the plasma power was pulsed ON and OFF, while applying a dc bias continuously, the tail of the EEPF extended to higher energies during the early active glow (shortly after plasma turn-ON). This effect was exacerbated near the sheath edge, where stochastic heating of electrons by the oscillating sheath was more prevalent. The corresponding time-average EED on the substrate surface had a distinct peak at an energy equivalent to the applied dc voltage. The time-average IED on the substrate was similar to that of the cw plasma, except for the presence of a prominent extra peak at very low ion energies (<10 eV). This peak was due to ions bombarding the substrate in the afterglow (when plasma power was OFF).

Depending on the system configuration, the application of a dc bias may lead to increased electron density. This can happen under conditions such as when: (a) values of NL (N = neutral gas density, L = interelectrode spacing) result in bounce resonance heating, whereby electrons accelerated by the sheath on one electrode, spend about half of the rf cycle traversing the plasma, only to capture the expansion of the sheath on the opposite electrode, and thus are heated efficiently, (b) the secondary electron beam intensity is of sufficient magnitude that two-stream instability results in excitation of electrostatic waves and ultimately in electron heating by Landau damping,[5,26] and/or (c) secondary electron emission by *electron* bombardment of the electrodes is important, depending on the electrode material and the impacting electron energy.

Notation

B = magnetic induction
E = electric field
f = distribution function
F = force on particle
m = electron mass
M = ion mass
n_e = electron density
n_i = ion density
q = charge on particle
s = time-average sheath thickness
t = time
V_{dc} = applied dc bias voltage
V_{rf} = peak voltage of applied rf power
V_s = time-average sheath voltage
v = particle velocity
x = spatial coordinate

Greek letters

τ_i = ion transit time through the sheath
τ_{rf} = period of plasma excitation rf signal
ν = plasma excitation frequency
$\omega = 2\pi\nu$ = plasma excitation angular frequency

Literature Cited

1. Lieberman MA, Lichtenberg AJ. Principles of Plasma Discharges and Materials Processing, 2nd ed. New York: Wiley-Interscience, 2005.

2. Report of the Department of Energy, Plasma Science: Not only the Fourth State of Matter but all of them, Office of Fusion Energy Sciences, Workshop on Low Temperature Plasmas, March 25–27, 2008.

3. Hamaoka F, Yagisawa T, Makabe T. Numerical investigation of relationship between micro-scale pattern, interfacial plasma structure and feature profile during deep-Si etching in two-frequency capacitively coupled plasmas in SF_6/O_2. *J Phys D: Appl Phys*. 2009;42:075201.

4. Kohler K, Coburn JW, Horne DE, Kay E, Keller JH. Plasma potentials of 13.56-MHz rf argon glow discharges in a planar system. *J Appl Phys*. 1985;57:59–66.

5. Xu L, Chen L, Funk M, Ranjan A, Hummel M, Bravenec R, Sundararajan R, Economou DJ, Donnelly VM. Diagnostics of ballistic electrons in a dc/rf hybrid capacitively coupled discharge. *Appl Phys Lett*. 2008;93:261502.

6. Kawamura E, Lichtenberg AJ, Lieberman MA. Secondary electrons in rf and dc/rf capacitive discharges. *Plasma Sources Sci Technol*. 2008;17:045002.

7. Kawamura E, Lieberman MA, Lichtenberg AJ, Hudson EA. Capacitive discharges driven by combined dc/rf sources. *J Vac Sci Technol A*. 2007;25:1456–1474.

8. Denpoh K, Ventzek PLG. Test particle simulation of the role of ballistic electrons in hybrid dc/rf capacitively coupled plasmas in argon. *J Vac Sci Technol A*. 2008;26:1415–1424.

9. Wang M, Kushner MJ. High energy electron fluxes in dc-augmented capacitively coupled plasmas I. *Fundamental characteristics*. *J Appl Phys*. 2010;107:023308.

10. Wang M, Kushner MJ. High energy electron fluxes in dc-augmented capacitively coupled plasmas. II. *Effects on twisting in high aspect ratio etching of dielectrics*. *J Appl Phys*. 2010;107:023309.

11. Jiang W, Xu X, Dai Z-L, Wang Y-N. Heating mechanisms and particle flow balancing of capacitively coupled plasmas driven by combined dc/rf sources. *Phys Plasmas*. 2008;15:033502.

12. Welch S, Keswick K, Stout P, Kim J, Lee W, Ying C, Doan K, Kim HS, Pu B. Advanced DRAMs drive: high-AR etch advances. *Semicond Int*. 2009;32:18–20.

13. Birdsall CK, Langdon AB. Plasma Physics via Computer Simulation. New York: McGraw-Hill, 1985.

14. Verboncoeur J, Alves MV, Vahedi V, Birdsall CK. Simultaneous potential and circuit solution for 1d bounded plasma particle simulation codes. *J Comput Phys*. 1993;104:321–328.

15. Vahedi V, Surendra M. A Monte Carlo collision model for the particle-in-cell method: applications to argon and oxygen discharges. *Comput Phys Commun*. 1995;87:179–198.

16. Vahedi V, DiPeso G. Simultaneous potential and circuit solution for two-dimensional bounded plasma simulation codes. *J Comput Phys*. 1997;131:149–163.

17. Phelps AV, Petrović ZLj. Cold-cathode discharges and breakdown in argon: surface and gas phase production of secondary electrons. *Plasma Sources Sci Technol*. 1999;8:R21–R44.

18. Diomede P, Longo S, Economou DJ, Capitelli M. Hybrid simulation of a dc-enhanced radio-frequency capacitive discharge in hydrogen. *J Phys D: Appl Phys*. 2012;45:175204.

19. Diomede P, Donnelly VM, Economou DJ. Particle-in-cell simulation of ion energy distributions on an electrode by applying tailored bias waveforms in the afterglow of a pulsed plasma. *J Appl Phys*. 2011;109:083302.

20. Nam SK, Economou DJ, Donnelly VM. Generation of fast neutral beams by ion neutralization in high-aspect-ratio holes: a Particle-in-Cell simulation study. *IEEE Trans Plasma Sci*. 2007;35:1370–1378.

21. Kawamura E, Vahedi V, Lieberman MA, Birdsall CK. Ion energy distributions in rf sheaths; review, analysis and simulation. *Plasma Sources Sci Technol*. 1999;8:R45–R64.

22. Panagopoulos T, Economou DJ. Plasma sheath model and ion energy distribution for all radio frequencies. *J Appl Phys*. 1999;85:3435–3443.

23. Edelberg EA, Aydil ES. Modeling of the sheath and the energy distribution of ions bombarding rf-biased substrates in high density plasma reactors and comparison to experimental measurements. *J Appl Phys*. 1999;86:4799–4812.

24. Wild C, Koidl P. Ion and electron dynamics in the sheath of radio-frequency glow discharges. *J Appl Phys*. 1991;69:2909–2922.

25. Zeuner M, Neumann H, Meichsner J. Ion energy distributions in a dc biased rf discharge. *J Appl Phys*. 1997;81:2985–2994.

26. Rose DV, Guillory JU, Beall JH. Comparison of particle-in-cell simulations and a wave-population model of electron-beam-plasma interactions. *Phys Plasmas*. 2002;9:1000–1009.